Research Square

Preprints are preliminary reports that have not undergone peer review.
They should not be considered conclusive, used to inform clinical practice,
or referenced by the media as validated information.

Dynamic Analysis and Reliability Prediction of Wind Turbine Gearbox Under Uncertain Excitation Conditions

Kamel Abboudi
University of Sfax
Mohanad Bahshwan
University of Jeddah
Sami Ghazali
University of Jeddah
Ahmed Ghorbel
University of Kairouan
Abdulmalik Alkotami
University of Jeddah
Ali Mkaddem
University of Jeddah
Abdessalem Jarraya
ajarraya@uj.edu.sa
University of Jeddah
Mohamed Haddar
University of Sfax

Article

Keywords: wind turbine, dynamic responses, reliability, gearbox

Posted Date: November 2nd, 2026

DOI: https://doi.org/10.21203/rs.3.rs-11265749/v1

License: This work is licensed under a Creative Commons Attribution 4.0 International License.
Read Full License

Additional Declarations: No competing interests reported.

Dynamic Analysis and Reliability Prediction of Wind Turbine Gearbox Under Uncertain Excitation Conditions

Kamel Abboudi[1,3], Mohanad Bahshwan[2], Sami Ghazali[2], Ahmed Ghorbel[1,4], Abdulmalik Alkotami[2], Ali Mkaddem[2], Abdessalem Jarraya[*1,2], Mohamed Haddar[1]

[1] Laboratory of Mechanics, Modelling and Production, National School of Engineering of Sfax, University of Sfax, Tunisia.
[2] Department of Mechanical and Materials Engineering, FoE, University of Jeddah, P.O. Box 80327, Jeddah 21589, Saudi Arabia.
[3] Preparatory Institute for Engineering Studies of Kairouan, University of Kairouan, Tunisia.
[4] Higher Institute of Applied Sciences and Technology of Kairouan, University of Kairouan, Tunisia.

*Corresponding author: *ajarraya@uj.edu.sa*

Abstract

Wind turbine drivetrains experience variable aerodynamic loads, which can significantly impact their dynamic response and reliability. This study investigates how uncertainty in wind speed and inflow angle propagates from aerodynamic loading to gearbox failure risk and drivetrain dynamics. A blade-element aerodynamic model will be coupled with a probabilistic torque-based limit-state formulation. This will be done using first- and second-order reliability methods and Monte Carlo simulation for reliability assessment. The resulting critical aerodynamic conditions will be applied to a five-inertia torsional model that represents a multistage gearbox with a planetary stage, two parallel gear stages, and flexible shafts. We hypothesize that aerodynamic uncertainty is the only factor that significantly influences failure probability, and that critical aerodynamic conditions produce increased torsional and speed fluctuations in the drivetrain.

Keywords: wind turbine; dynamic responses; reliability; gearbox.

List of symbols

δL lift elementary force, N;	μ_G mean value of the function G;
δD drag elementary force, N;	σ_G standard deviation of the function G;
V_{rel} relative wind, m/s^2;	n_b number of blades;
U wind speed, m/s^2;	D rotor diameter, m;
v blade speed, m/s^2;	ρ air density, kg/m^3;
V_w wake rotation at the rotor plane, m/s^2;	J_{turb} inertia of rotor, kg·m^2;
V_T thrust speed, m/s^2;	$J_{carrier}$ inertia of planet carrier, kg·m^2;

$\mathbf{V_i}$ induced speed, m/s^2;

c(r) chord length in the distance r from the rotor axis;

$\mathbf{C_L}$ Lift coefficient;

$\mathbf{C_D}$ drag coefficient;

ϕ inflow angle, deg;

$\boldsymbol{\eta}$ aerodynamic efficiency of airfoil;

G limit state function;

T Rosenblatt function;

$\mathbf{F_{Xi}}$ marginal cumulative distribution function of X_i;

$\boldsymbol{\Phi}$ cumulative distribution function of the standard normal distribution;

$\boldsymbol{\beta}$ reliability index;

$\mathbf{P_f}$ probability of failure;

$\mathbf{J_{planet}}$ inertia of planet gear, kg·m^2;

$\mathbf{J_{sun}}$ inertia of sun gear, kg·m^2;

$\mathbf{J_i; i=4…7}$ parallel gear inertia, kg·m^2 (resp.);

$\mathbf{J_{gen}}$ inertia of generator, kg·m^2;

$\mathbf{k_{RS}}$ stiffness of low speed shaft, Nm/degree;

$\mathbf{k_2}$ stiffness of first intermediate shaft, Nm/degree;

$\mathbf{k_3}$ stiffness of second intermediate shaft, Nm/degree;

$\mathbf{k_{GS}}$ stiffness of high speed shaft, Nm/degree;

$\mathbf{B_{RS}}$ damping of low speed shaft, Nm/(rev/min);

$\mathbf{B_2}$ damping of first intermediate shaft, Nm/(rev/min);

$\mathbf{B_3}$ damping of second intermediate shaft, Nm/(rev/min);

$\mathbf{B_{GS}}$ damping of high speed shaft, Nm/(rev/min);

$\mathbf{Z_{ring}, Z_{planet}, Z_{sun}, Z_1 … Z_4}$ Ring , Planet, Sun, gears 1…4;

Introduction

Wind energy has become an important component of the global transition toward sustainable and low-carbon energy systems. Its economic competitiveness, technological maturity, and large-scale deployment have contributed to the continuous development of increasingly powerful and complex wind turbines [1]. Recent reports have further highlighted the growing role of wind power in the global energy mix and the need to improve the reliability and availability of wind energy conversion systems [2,3]. As wind turbines continue to increase in size and power rating, their mechanical transmission systems are subjected to increasingly demanding operating conditions.

The drivetrain is a critical subsystem of a wind turbine, transmitting the aerodynamic torque generated by the rotor to the electrical generator while increasing the rotational speed to the required operating level [4]. Among its components, the gearbox is particularly vulnerable because it is continuously subjected to variable torque, torsional oscillations, and transient aerodynamic loads. The stochastic nature of wind excitation can generate significant dynamic loads and accelerate fatigue damage in gears, shafts, bearings, and other drivetrain components [5,6]. Consequently, accurate prediction of drivetrain dynamics and reliable assessment of gearbox performance are essential for improving turbine availability, reducing maintenance costs, and preventing unexpected failures [7,8]. Recent reviews have also emphasized that the reliability of wind turbine gearboxes remains a challenging issue, particularly when the effects of uncertain wind loading and multiple interacting failure mechanisms are considered [5].

Over the past decades, numerous dynamic models have been developed to describe the behavior of wind turbine drivetrains. These models range from simplified equivalent single- or two-mass representations to more detailed multi-degree-of-freedom and flexible multibody formulations [9,10]. Although reduced-order models are computationally attractive, they may not adequately reproduce the torsional interactions generated within multistage gear transmissions. Multi-mass models therefore remain widely used to investigate torsional vibration, resonance, load transmission, and dynamic load sharing in wind turbine gearboxes [11, 13]. In particular, Abboudi et al. [13] investigated the dynamic behavior of a two-stage gear train subjected to wind turbine operating conditions, while more recent studies have addressed

reliability-based design and optimization of wind turbine gearboxes [14]. Chen et al. [15] further demonstrated the importance of considering electromechanical and rigid-flexible coupling effects in the dynamic analysis of wind turbine transmission systems. Other investigations have considered non-torque loads [10], bevel gear dynamics [12], flexible multibody behavior [17], and advanced control strategies under variable operating conditions [18, 20].

Despite these developments, a significant part of the existing literature remains based on deterministic operating conditions. Such approaches generally assume prescribed wind loads and nominal system parameters, although actual wind turbine operation is inherently uncertain. Wind speed, flow direction, turbulence, aerodynamic coefficients, and structural properties may exhibit substantial variability, which can strongly affect both the aerodynamic torque and the dynamic response of the drivetrain [21, 24]. Tounsi et al. [22], for example, demonstrated the influence of aerodynamic uncertainty on the dynamic response of a two-stage gear system, while Hadj Kacem et al. [23] investigated the effect of multiple uncertainties on the dynamics of a wind turbine gearbox using generalized polynomial chaos. Similarly, uncertainty in wind speed has been shown to play an important role in the prediction of wind turbine behavior [24]. More recent studies have continued to emphasize the importance of uncertainty quantification in gearbox dynamics and reliability assessment [25, 26, 27, 28]. Du et al., for instance, investigated the dynamic response of a multistage wind turbine transmission system under uncertain aerodynamic loading, demonstrating that load-related uncertainties can significantly affect the predicted dynamic behavior [29].

Reliability-based approaches provide a complementary perspective by transforming uncertain operating conditions into quantitative measures of failure probability and reliability. FORM and SORM are particularly attractive for engineering applications because they can estimate failure probabilities with substantially lower computational costs than direct Monte Carlo Simulation, while MCS remains an important reference technique for validating probabilistic predictions [8,25]. Recent research has increasingly focused on reliability assessment of wind turbine gearboxes under random wind loading, including component-level fatigue reliability, failure correlation, and system-level reliability degradation [5,30]. However, these studies often focus primarily on statistical failure modeling or component reliability and do not explicitly establish a direct link between the critical aerodynamic conditions identified through reliability analysis and the resulting torsional dynamics of a multistage drivetrain. Conversely, dynamic studies frequently characterize vibration and load transmission without quantifying the probability of reaching critical operating conditions.

This gap motivates the development of a coupled probabilistic–dynamic framework capable of connecting uncertain aerodynamic excitation, gearbox dynamic behavior, and system reliability within a unified methodology. In particular, identifying the most probable combination of wind parameters leading to a limit state can provide physically meaningful loading conditions for subsequent dynamic analysis. Such an approach makes it possible not only to estimate the probability of failure but also to investigate the mechanical response of the drivetrain when operating near critical conditions.

Accordingly, the present study proposes an integrated aerodynamic, dynamic, and reliability framework for a multistage wind turbine transmission system. The aerodynamic torque is determined as a function of wind speed and inflow angle, which are considered the principal uncertain environmental parameters. A torque-based limit-state function is then formulated to identify critical operating conditions using FORM and SORM, while Monte Carlo Simulation is employed as an independent reference. The resulting critical aerodynamic conditions are subsequently introduced into a lumped-parameter dynamic model incorporating a planetary gearbox stage, parallel gear stages, and flexible drivetrain shafts. The resulting torsional response, rotational-speed fluctuations, and modal characteristics are analyzed to establish the relationship between aerodynamic uncertainty and drivetrain dynamics. The main contribution of this work is therefore the direct coupling of probabilistic identification of critical wind conditions with the dynamic assessment of the gearbox, providing a physically consistent framework for evaluating both failure probability and mechanical response under unfavorable operating conditions.

Wind turbine system

As shown in Figure 1, the wind turbine model comprises three main subsystems: the aerodynamic rotor; the mechanical kinematic chain; and the electrical system, which is represented by the generator. The mechanical subsystem comprises the rotor shaft, the generator shaft and a multistage gearbox.

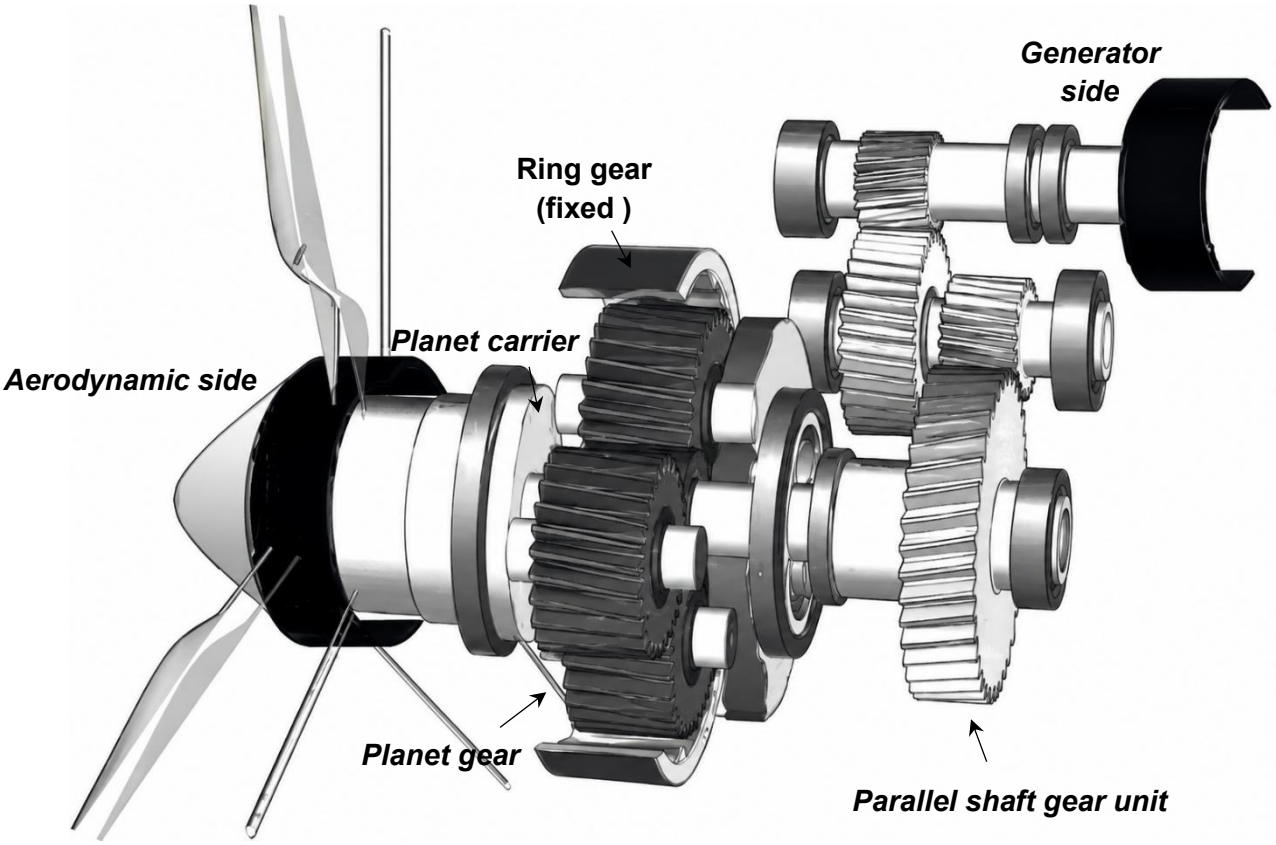


Fig 1. Line schematic of the mechanical transmission in wind turbine system.

Planetary gear trains are generally used for the low-speed stage in the gearboxes of modern wind turbines because of their advantageous dynamic properties. One of the main advantages of planetary gears is their ability to reduce vibration transmission to the nacelle and tower, since the torque is distributed across three planetary gears, which tend to balance each other's reaction forces out.

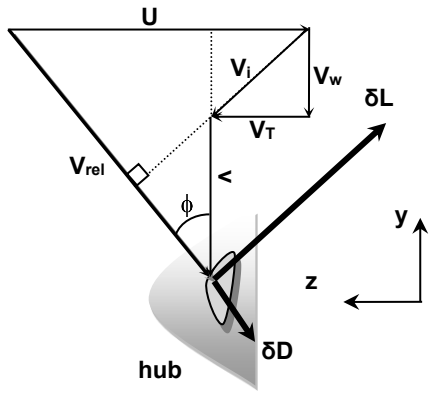
In this study, we consider a simplified mechanical model consisting of a planetary (epicyclic) stage followed by two helical gear stages. The planetary system comprises a planet carrier (2) that supports three identical, equidistant planets (4), while the outer ring gear (5) remains fixed.

Aerodynamic torque modelling

The system is primarily excited by wind, so the uncertainty of this excitation is represented by two influential parameters: wind speed magnitude and wind direction. The aerodynamic torque was expressed as a function of these two uncertain input variables using an aerodynamic model that was developed accordingly. This torque is then introduced into the system's dynamic model, enabling wind-

induced uncertainties to propagate towards the structural or mechanical response and, ultimately, towards the failure criterion.

This study considers a three-bladed, variable-speed wind turbine with a rated power of 1.5 MW and a rotor radius of 36 metres. This corresponds to a rotor diameter of 72 metres. It is assumed that the hub diameter is 4 metres and that the blade root is located at the hub surface.



Fig; 2. Speed triangle seen locally on a blade.

Zalkind et al. [5] and Abboudi et al. [13] explain how to calculate the two aerodynamic forces, δL and δD, acting on each cross-sectional element of the wing. δL is the elementary lift force normal to the relative wind direction, V_{REL}. δD is the elementary drag force parallel to the relative wind, V_{rel}.

Figure 2 shows two velocity triangles (wind speed U, blade speed v, and resultant speed V_{rel}) and (inflow speed caused by wake rotation at the rotor plane V_w, thrust speed V_T, and induced speed V_i) at the blade mid radius.

The first part aims to determine the critical aerodynamic conditions that could cause the wind turbine to reach its limit state. Two variables that directly influence the aerodynamic forces generated by the blades, and consequently the aerodynamic torque transmitted to the gearbox, were selected: the first characterizes the absolute wind speed denoted by U, and the second characterizes its direction, i.e. the angle of attack denoted by ϕ.

In order to achieve this goal, we first need to determine the lift and drag forces δL and δD exerted on one blade element with thickness δr.

$$\delta L = 0.5\rho C_L V_{rel}^2 c(r)\delta r \tag{1}$$

And drag forces is

$$\delta D = 0.5\rho C_D V_{rel}^2 c(r)\delta r \tag{2}$$

We calculate the lift and drag coefficients using the aerodynamic model that Lanzafame and Messina proposed [16]. A wide range of angles of attack are covered by the model's consistent representation of

the aerodynamic coefficients, which includes attached-flow, high-lift and stall-development, and fully stalled regimes.
It is expressed as follows:

$$C_L = \begin{cases} \sum_{i=0}^{5} \left[a_i \ln(\alpha+\gamma) \right]^i; & -6° \le \alpha \le 20° \\ 2C_{L,max} \sin(\alpha)\cos(\alpha); & 20° \le \alpha \le 45° \end{cases} \quad (3)$$

$$C_D = \begin{cases} \sum_{i=0}^{5} \left[b_i \ln(\alpha+\gamma) \right]^i; & -6° \le \alpha \le 20° \\ C_{D,max} \sin^2(\alpha); & 20° \le \alpha \le 45° \end{cases} \quad (4)$$

Where,
The attack angle, denoted by α, is the difference between the incident angle, ϕ, and the twist angle, γ.

$$\alpha = \phi - \gamma \quad (5)$$

The coefficients a_i and b_i are determined by applying a least-squares procedure to the experimental airfoil data [16].

As can be seen from Figure 2, the relative wind speed is:

$$V_{rel} = \frac{U}{\sin\phi} \quad (6)$$

The elementary aerodynamic torque, generalized to the three blades (noted n_b) is:

$$T_{aero}(U,\varphi) = \frac{n_b \rho U^2}{2} \left(4C_{L,max} - C_{D,max} \right) \int_{r_{hub}}^{r_{tip}} c(r)\cos(\phi-\gamma) r \delta r \quad (7)$$

r_{hub} and r_{tip} are respectively the hub radius and the overall blade radius (tip distance from the hub center).

The chord line for each spanwise section is noted c(r).

The reliability analysis of the aerodynamic torque using FORM and SORM is the focus of the second part of this study. The MPP is determined based on the defined limit-state function in order to identify the critical combination of the uncertain parameters U* and ϕ* using the defined limit-state function. The critical torque T_{lim}= T_{aero} (U*, ϕ *) represents the aerodynamic loading at the most probable failure point (MPP), and is then used to evaluate the system's reliability.

Probability and Reliability Methods

The probabilistic analysis primarily aims to determine the probability of failure and the associated reliability index, β, to identify critical combinations of uncertain wind parameters that correspond to the most probable failure conditions. Specifically, absolute wind speed and angle of incidence characterize

wind intensity and orientation, respectively. The critical values of these parameters are determined at or near the design point on the limit-state surface using the FORM and SORM approaches. The critical wind conditions are then introduced into the aerodynamic model to calculate the corresponding aerodynamic torque. This torque is then applied to the dynamic model of the wind turbine transmission system. This procedure allows for the investigation of the dynamic behavior of the gearbox under critical wind loading conditions and the identification of the mechanical response associated with the onset of failure. Monte Carlo Simulation is finally used to provide a reference. This reference is used to assess the accuracy and consistency of the estimated failure probability and reliability index.

In order to prevent damage to the blades and mechanical transmission components, the wind turbine must operate within safe limits. This is because the turbine is driven by an uncontrollable energy source. The extracted torque (T_{aero}) from the wind is the control variable that can be adjusted. The first step is to identify the factors that influence it: wind speed (U) and wind direction relative to the blades (ϕ). The limit state function, $G(U, \phi)$, is the difference between the rated torque value, T_{lim}, and the extracted power, T_{aero}. The function is given by:

$$G(U,\phi) = T_{lim} - T_{aero}(U,\phi) \tag{8}$$

In the aerodynamic modeling, two uncertain parameters appear: absolute wind speed variable, U, and inflow angle ϕ. These stochastic parameters are replaced by X_1 and X_2 respectively;

$$G(X_1,X_2) = T_{lim} - \frac{3\rho U^2}{2}\left(4C_{L,max} - C_{D,max}\right)\int_{r_{hub}}^{r_{tip}} c(r)\cos\left(\phi-\gamma\right)r\delta r \tag{9}$$

In other words, once we have determined the performance function, the stochastic parameters must be transformed from originally random design space to the standard normal design space (Gaussian space) by Rosenblatt function T:

$$\left(X_1,X_2\right)\xrightarrow{T}\left(Z_1,Z_2\right)$$

$$T:\begin{cases} Z_1 = \Phi^{-1}\left[F_{X_1}\left(X_1\right)\right] \\ Z_2 = \Phi^{-1}\left[F_{X_2}\left(X_2\right)\right] \end{cases} \tag{10}$$

Where,

F_{X_i} is the marginal cumulative distribution function of X_i.

$\Phi(.)$ is the cumulative distribution function of the standard normal distribution.

The probability of failure can be clearly defined in terms of occurrence of a failure. The FORM/SORM methods are used to approximate this probability. It should be noted that the second method uses the results of the first method. (Chen et al. [15])

The probability of failure can be written as:

$$P_f\left(G(X_1,X_2)\le 0\right)=\int_{G(X_1,X_2)\le 0} f_x(X)dx \tag{11}$$

Eq. (11) is transformed into the following integration:

$$\begin{aligned} P_f\left(G(Z_1,Z_2)\le 0\right) &\cong \Phi(-\beta) \\ &= \iint_{G(Z_1,Z_2)\le 0} \prod_{i=1}^{2}\frac{1}{\sqrt{2\pi}}\exp\left(-\frac{1}{2}z_i{}^2\right)dz_1dz_2 \end{aligned} \tag{12}$$

The reliability index can be found by equation:

$$\beta=-\Phi^{-1}(P_f) \tag{13}$$

The first method based on the first-order Taylor series approximation of a limit state function yields the following expression.

$$G(Z)=G(z^*)+\left(\frac{\partial G(Z)}{\partial Z_1},\frac{\partial G(Z)}{\partial Z_2}\right)_{|z^*}(Z-z^*)^T \tag{14}$$

Where z* are the coordinates of the design point in the Z-space

$$\begin{aligned} P_f(G(Z_1,Z_2)\le 0) &\cong \Phi\left(-\frac{\mu_G}{\sigma_G}\right) \\ &= \Phi\left(\frac{-\sum_{i=1}^{2}\frac{\partial G(Z)}{\partial Z_i}_{|z^*}.z^*}{\sqrt{\left(\sum_{i=1}^{2}\frac{\partial G(Z)}{\partial Z_i}_{|z^*}\right)^2}}\right) \end{aligned} \tag{15}$$

In the SORM approach, the probability of failure is given by:

$$P_f(G(Z_1,Z_2)\le 0)\cong\Phi(-\beta)\prod_{i=1}^{n}(1-k_i\beta)^{-1/2} \tag{16}$$

Where k_i are the different individual curvatures at the design point.

Finally, Monte Carlo simulation (MCS) was used as a reference method to estimate the probability of failure independently and to evaluate the accuracy of the reliability results obtained using FORM and SORM.

Hence, the failure probability can be estimated with:

$$P_f\left(G\left(Z_1,Z_2\right)\le 0\right)\cong\frac{1}{N}\sum_{k}^{N}I\left[G(Z_i)<0\right] \tag{17}$$

Where, N is total number of Monte Carlo samples.

The Indicator function leads to next condition:

$$I\left[G(Zi)\right]=\begin{cases}1 & \text{If } G(Z_i)<0\\ 0 & \text{If } G(Z_i)\ge 0\end{cases} \tag{18}$$

Dynamic modelling of a multistage gearbox

In this section, we examine the gear transmission system of a 1.5 MW wind turbine, paying particular attention to the impact of shaft flexibility, especially that of the high-speed and low-speed shafts, as well as the intermediate shafts, on the modal characteristics of the entire system. The inertias (J_{Turb}, $J_{2,3}$, J_4, J_5,J_6, J_7, J_{Gen}) represent the rotational inertia of the main drivetrain components, including the wind turbine rotor, planetary carrier, pinions and generator. The torsional stiffness models (K_{RS},K_2,K_3,K_{GS}) represent the elastic behaviour of the corresponding shafts, characterized by their resistance to torsional deformation. Furthermore, the viscous damping coefficients (B_{RS}, B_2, B_3, B_{GS}) account for energy dissipation resulting from friction and internal losses within the transmission system.

In order to reduce computational complexity while preserving the transmission system's main torsional dynamic characteristics, a reduced-order modelling approach was adopted. Equivalent inertias ($J_{2,3}$, $J_{4,5}$ and $J_{6,7}$) replaced three groups of inertial elements, while the wind turbine rotor inertia and the generator rotor inertia were kept explicitly. As a result, the original eight-inertia system was simplified to a five-inertia lumped-parameter model.

The model takes into account the torsional flexibility of the shafts, which is the main source of dynamic compliance. Other local flexibilities, such as tooth flexibility or uncoupled shaft bending, are considered negligible in this modal analysis of the gear train.

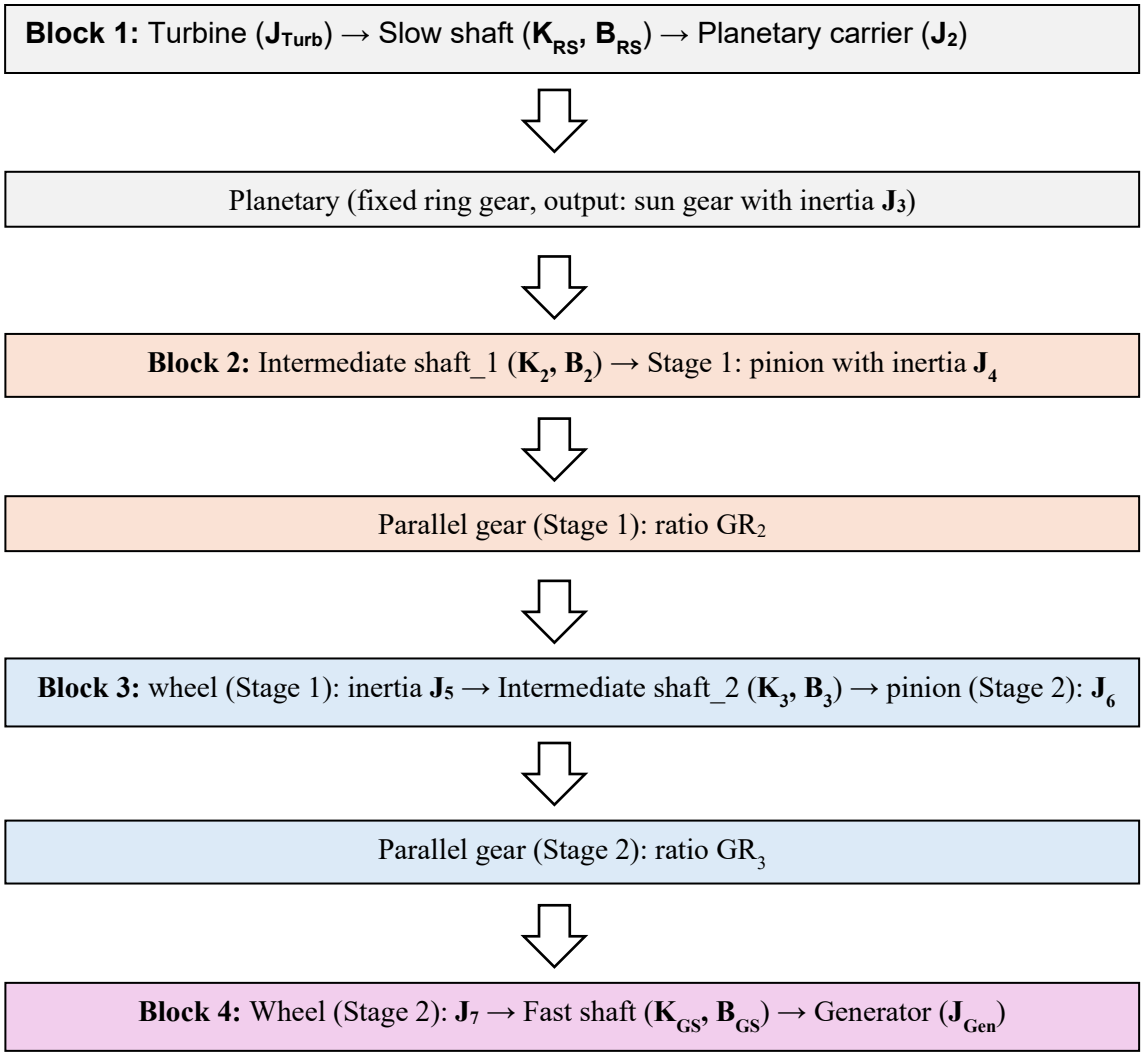


Figure 3. Structure diagram of the studied wind turbine.

The gear ratio of the planetary gear (for ring fixed, sun driving and career output):

$$GR_1 = 1 + \frac{Z_{ring}}{Z_{sun}} \tag{19}$$

The parallel stage ratios describe the individual transmission ratios associated with each parallel gear stage within the drivetrain, reflecting how motion is distributed and recombined through the gear meshes; whereas e_2 and e_3 are the gear ratios of the first and second parallel gear stages, respectively.

$$GR_2 = \frac{Z_4}{Z_5} \tag{20}$$

$$GR_3 = \frac{Z_6}{Z_7} \tag{21}$$

The total ratio is obtained by combining the global gear ratio with the parallel stage ratios, and it represents the effective transmission ratio of the complete gearbox from input to output.

$$\mathrm{GR}_{\mathrm{total}} = \prod_{\mathrm{i}=1}^{3} \mathrm{GR}_{\mathrm{i}}$$

(22)

The generator torque is related to the mechanical torque transmitted through the gearbox via the total gear ratio and transmission efficiency. Specifically, the torque at the generator shaft is obtained by scaling the turbine-side torque by the reciprocal of the total gear ratio $\mathrm{GR}_{\mathrm{total}}$, taking into account losses in the drivetrain η_{total}.

$$\mathrm{T}_{\mathrm{gen}} = -\frac{\mathrm{T}_{\mathrm{turb}}\left(\mathrm{U}^{*}(\mathrm{t}), \phi^{*}\right)}{\mathrm{GR}_{\mathrm{total}} \cdot \eta_{\mathrm{total}}} \tag{23}$$

We propose a linearized multi-body model of a wind turbine gearbox, expressed in the form of matrix differential equations, to represent the mechanical transmission chain. Unlike a conventional kinematic model, this model takes into account dynamic effects such as oscillations, damping and stiffness. The state space formulation is as follows:

$$\dot{\mathrm{x}}(\mathrm{t}) = \mathrm{A}\mathrm{x}(\mathrm{t}) + \mathrm{B}\mathrm{u}(\mathrm{t}) \tag{24}$$

The state vector for an eight-inertia torsional drivetrain (e.g. rotor, planetary carrier, sun gear, parallel gear inertias and generator) is as follows:

$$\mathrm{x}(\mathrm{t}) = \begin{bmatrix} \Omega(\mathrm{t}) \\ \mathrm{T}_{\mathrm{in}}(\mathrm{t}) \end{bmatrix} \tag{25}$$

The five generalized angular velocities $\Omega(\mathrm{t}) = \begin{bmatrix} \Omega_1 & \Omega_2 & \Omega_3 & \Omega_4 & \Omega_5 \end{bmatrix}^{\mathrm{T}}$ represent the rotational motion of the five equivalent inertial blocks that constitute the reduced wind turbine drivetrain. We can obtain the equivalent inertias by combining the inertial contributions of the intermediate drivetrain components according to the corresponding gear ratios.

$\mathrm{T}_{\mathrm{in}}(\mathrm{t}) = \begin{bmatrix} \mathrm{T}_{12} & \mathrm{T}_{34} & \mathrm{T}_{56} & \mathrm{T}_{78} \end{bmatrix}^{\mathrm{T}}$: contains the internal torsional torques between adjacent bodies.

$\mathrm{u}(\mathrm{t}) = \begin{bmatrix} \mathrm{T}_{\mathrm{aero}}\left(\mathrm{U}^{*}(\mathrm{t}), \phi^{*}\right), & \mathrm{T}_{\mathrm{gen}} \end{bmatrix}$ is the inputs which contain the external mechanical torques such as wind torque at the rotor and electromagnetic torque at the generator.

Matrix $\mathrm{A} \in \mathrm{R}^{9\times9}$: describes the coupled differential equations (angular velocities and internal torques).

$$A=\begin{bmatrix} 0 & a_{1,2} & 0 & 0 & 0 & 0 & 0 & 0 & 0 \\ a_{2,1} & a_{2,2} & a_{2,3} & a_{2,4} & 0 & 0 & 0 & 0 & 0 \\ 0 & a_{3,2} & 0 & a_{3,4} & 0 & 0 & 0 & 0 & 0 \\ 0 & a_{4,2} & a_{4,3} & a_{4,4} & a_{4,5} & a_{4,6} & 0 & 0 & 0 \\ 0 & 0 & 0 & a_{5,4} & 0 & a_{5,6} & 0 & 0 & 0 \\ 0 & 0 & 0 & a_{6,4} & a_{6,5} & a_{6,6} & a_{6,7} & a_{6,8} & 0 \\ 0 & 0 & 0 & 0 & 0 & a_{7,6} & 0 & a_{7,8} & 0 \\ 0 & 0 & 0 & 0 & 0 & a_{8,6} & a_{8,7} & a_{8,8} & a_{8,9} \\ 0 & 0 & 0 & 0 & 0 & 0 & 0 & a_{9,8} & 0 \end{bmatrix} \quad (26)$$

Matrix $B \in R^{9\times 2}$: applies the external inputs (turbine torque T_{turb} and generator torque T_{gen}.

$$B=\left[a_{1,2},\quad a_{1,2}B_1,\quad \text{zeros}(1,7);\quad \text{zeros}(1,8),\quad -a_{9,8}\right]^T \quad (27)$$

Table 1: Term ($a_{k,m}$), where "k" denotes row index and "m" denotes the column index.

$a_{1,2}=-\frac{1}{J_{Turb}}$	$a_{2,1}=k_{RS}$	$a_{2,2}=-B_{RS}\left(\frac{1}{J_{Turb}}+\frac{1}{J_2}\right)$
$a_{2,3}=k_{RS}$	$a_{2,4}=\left(\frac{B_{RS}}{J_2}\right).GR_1$	$a_{3,4}=-GR_1.a_{3,2}=-GR_1.\left(\frac{1}{J_2}\right)$
$a_{4,2}=\left(\frac{B_2}{J_2}\right).GR_1$	$a_{4,3}=k_2.GR_1$	$a_{4,4}=-\left(\frac{B_2}{J_2}\right).GR_1^2-\frac{B_2}{J_4}$
$a_{4,5}=-k_2$	$a_{4,6}=\left(\frac{B_2}{J_4}\right).GR_2$	$a_{5,4}=-a_{5,4}.GR_2=-\left(\frac{1}{J_4}\right).GR_2$
$a_{6,4}=\left(\frac{B_3}{J_4}\right).GR_2$	$a_{6,5}=k_3.GR_2$	$a_{66}=-\left(\frac{B_3}{J_4}\right).GR_2^2-\frac{B_3}{J_6}$
$a_{67}=-k_3$	$a_{68}=\left(\frac{B_3}{J_6}\right).GR_3$	$a_{7,6}=\frac{1}{J_6}$
$a_{7,8}=-GR_3.a_{7,6}$	$a_{8,6}=\left(\frac{B_{GS}}{J_6}\right).GR_3$	$a_{8,7}=k_{GS}.GR_3$
$a_{8,8}=-\left(\frac{B_{GS}}{J_6}\right).GR_3^2-\frac{B_{GS}}{J_{Gen}}$	$a_{8,9}=k_{GS}$	$a_{9,8}=\frac{1}{J_{Gen}}$

The values used for all variables can be found in table 2

Table 2. Used numerical variables.

Parameter and symbol	Value / Units
number of blades, n_b	3
rotor diameter, D	72 m
air density, ρ	1.22 kg/m^3
inertia of rotor, J_{turb}	$4.8 \cdot 10^6$ kg·m^2
inertia of planet carrier, J_C	80 kg·m^2
inertia of planet gear, J_P	5 kg·m^2
inertia of sun gear, J_s	10 kg·m^2
parallel gear inertia, J_i; i=1…4	8,3,7,3 kg·m^2 (resp.)
inertia of generator, J_{gen}	200 kg·m^2
stiffness of low speed shaft, k_{RS}	$1.79 \cdot 10^6$ Nm/degree
stiffness of first intermediate shaft, k_2	488000 Nm/degree
stiffness of second intermediate shaft, k_3	360000 Nm/degree
stiffness of high speed shaft, k_{GS}	42000 Nm/degree
damping of low speed shaft, B_{RS}	25000 Nm/(rev/min)
damping of first intermediate shaft, B_2	20000 Nm/(rev/min)
damping of second intermediate shaft, B_3	15000 Nm/(rev/min)
damping of high speed shaft, B_{GS}	12000 Nm/(rev/min)
Ring , Planet, Sun, gears 1…4 (Z_{ring}, Z_{planet}, Z_{sun}, Z_1… Z_4)	99, 39, 21, 82, 23, 76, 23

Results and discussion

The aerodynamic model and the dependence of the aerodynamic torque on the uncertain wind parameters have been established. A reliability analysis is then performed using the first-order and second-order reliability methods (FORM and SORM). The aim is to find the most probable point (MPP) on the limit-state surface and evaluate the reliability index and failure probability associated with it. The critical aerodynamic torque $T_{lim}=T_{aero}(U^*,\phi^*)$ corresponding to the MPP is the ultimate goal. This is defined by the critical values of wind speed U* and incidence angle ϕ*.

As shown in Figure 10, the safe and failure domains are defined by the limit-state function. The safe domain is characterized by $G(X_1, X_2) > 0$, whereas failure occurs when $G(X_1, X_2) < 0$. The limit-state boundary is defined by $G(X_1, X_2) = 0$. The MPP is located at approximately $X_1^*=U^* \approx 11$ m/s and $X_2^* = \phi^* \approx 16°$. As this incidence angle is proximate to the 20° threshold that differentiates the combined attached/high-lift regime from the fully stalled regime in the adopted aerodynamic model, the MPP signifies that the critical operating condition is attained in the proximity of the onset of the fully stalled regime.

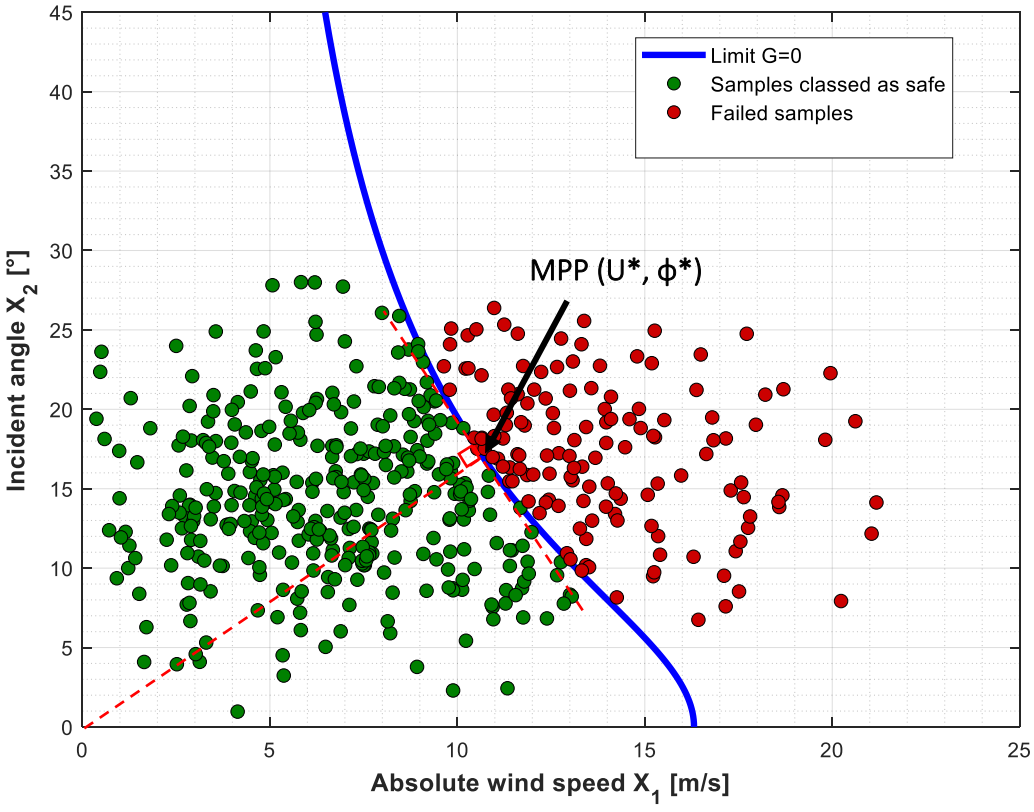


Fig. 4. Two parts of reliability model (MPP: U*≈11 m/s ϕ*≈16 deg)

The two-dimensional probability density map of equation (12) is shown in Figure 5, plotted on the X_1-X_2 plane. This shows the spatial distribution of the joint probability density function, $f_{X1\text{-}X2}(x)$, while the limit-state curve, $G(X_1, X_2)=0$, separates the safe domain (G>0) from the failure domain (G<0). The most

probable point (MPP) is located on this boundary. It corresponds to the most likely critical combination of random variables. This combination leads to the limit state. This graphical representation clearly shows the relative positions of the high-probability regions in relation to the failure boundary.

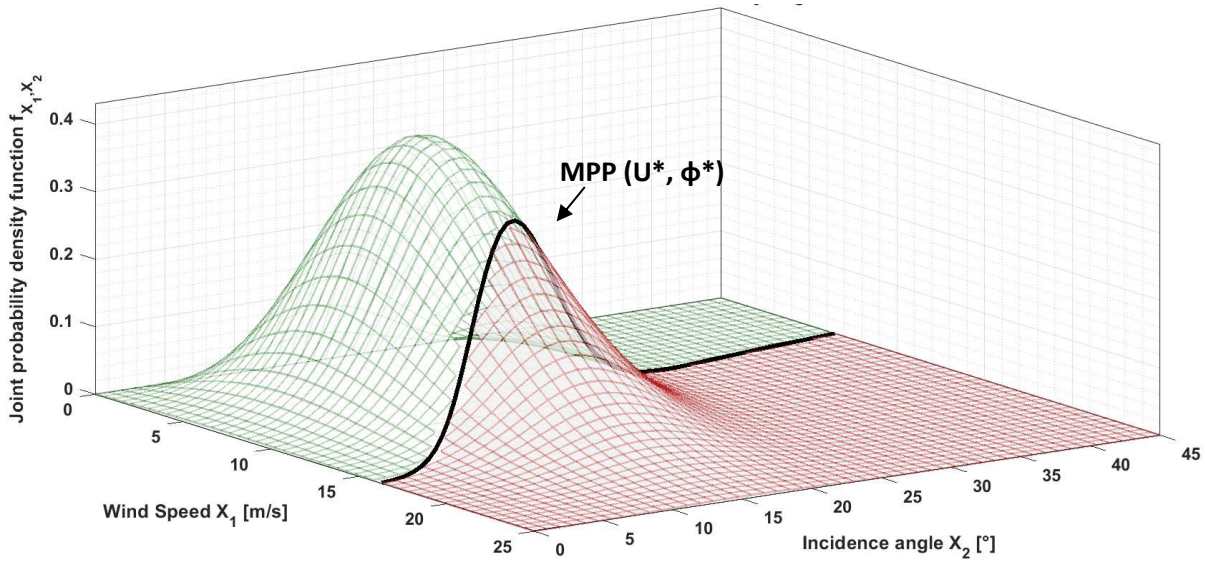


Fig. 5. 3D Joint distribution and Failure/Safety regions.

Table 3. Reliability index and probability of failure according to different distribution cases.

		Reliability index (β)			**Probability of failure (P_f)**		
		FORM	**SORM**	**MC**	**FORM**	**SORM**	**MC**
Case 1	X1~N(13,3) ; X2~N(18,3)	2.1787	2.2647	2.1644	0.0146	0.0117	0.0147
Case 2	X1~N(11,3); X2~N(16,3)	0.9771	1.0855	0.8549	0.1642	0.1388	0.1563
Case 3	X1~N(13,3) ; X2~N(16,3)	2.0491	2.1283	2.1372	0.0202	0.0166	0.0145

The reliability indices and failure probabilities obtained using FORM, SORM and Monte Carlo (MC) simulation are compared in Table 3. It is evident that Case 2 is the most critical configuration. It has the lowest reliability index, ranging from β=0.8549 to 1.0855. It also has the highest failure probability, ranging from P_f=0.1388 to 0.1642. In contrast, Cases 1 and 3 exhibit significantly higher and comparable reliability levels. The MC results for Case 1 are β=2.1644 and P_f=0.0147, and for Case 3 they are β=2.1372 and

P_f=0.0145. Overall, the results obtained by FORM and SORM are in reasonable agreement with the MC simulations, which supports the applicability of these reliability methods to the proposed model.

The reliability analyses are based on a BEM model, in which the lift/drag coefficients are approximated using the Lanzafame and Messina formulations[16]. These authors have divided the aerodynamic behaviour into three regimes. Zone A is the attached-flow regime, Zone B is the high-lift and stall-development regime, and Zone C is the fully stalled regime. In the adopted formulation, the experimental aerodynamic data for Zones A and B are represented over the range $-6 \leq \phi \leq 20°$ using fifth-order logarithmic polynomial fits. The post-stall regime is modelled using flat-plate relations for $20° \leq \phi \leq 45°$.

The Maximum Power Point (MPP) for this 1.5 MW turbine is found at X_1=11 m/s and X_2=16°, which is in close proximity to the onset of the fully stalled regime. In this zone, the aerodynamic coefficients exhibit abrupt nonlinearities, such as a sharp drop in lift and a steep rise in drag, which makes the torque response highly sensitive to small variations in wind speed or incidence angle. The fig. 6 shows that the torque increases linearly with the incident angle up to approximately 10–12°, after which it decreases, indicating the onset of aerodynamic stall.

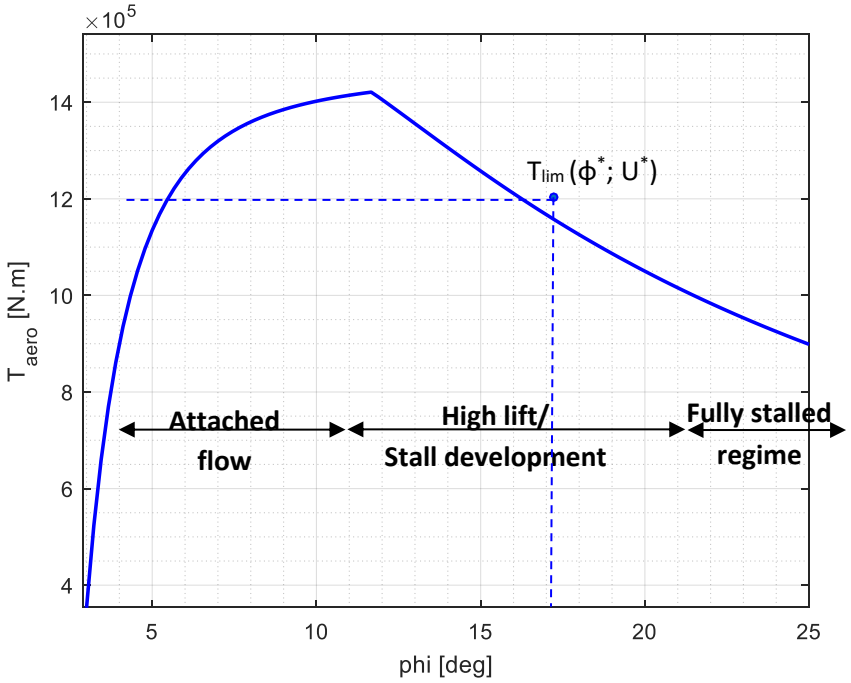


Fig. 6. Aerodynamic torque versus incident angle (U^*=11 m/s)

As shown in Figure 7, the actual operating conditions are accurately reflected by the variation in aerodynamic torque. The gearbox of the wind turbine drivetrain is particularly affected by this temporal variability, which directly impacts its dynamic response. The aerodynamic and reliability analyses were followed by an investigation into the dynamic behaviour of the gearbox under variable wind loading. The incidence angle is held constant while the absolute wind speed follows a normal distribution with a mean

of 11 m/s and a standard deviation of 3 m/s. The resulting aerodynamic torque is then used to excite the drivetrain model over time.

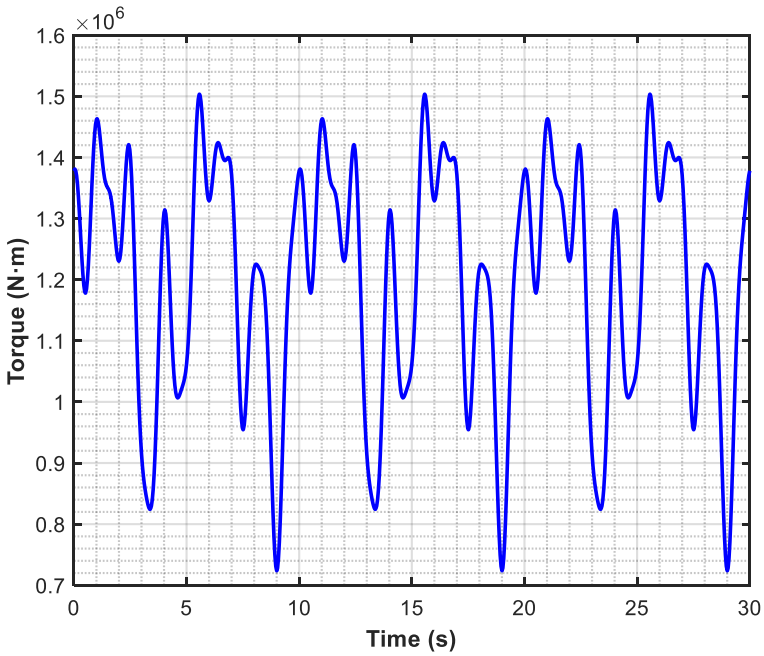


Fig. 7. Aerodynamic torque variation for a critical incidence angle of 16°.

The figures 8 and 9 show how angular velocity behaves differently in the blocks representing the low-speed input shaft and the output shaft connected to the generator. Angular velocity fluctuations at the input shaft remain low due to the high inertia of the powertrain components, which filter out aerodynamic disturbances effectively. In contrast, the output shaft exhibits more pronounced fluctuations, primarily due to its low inertia. This increased sensitivity underscores the necessity of control and damping strategies to maintain a nearly constant angular velocity on the generator side, ensuring stable and efficient power generation.

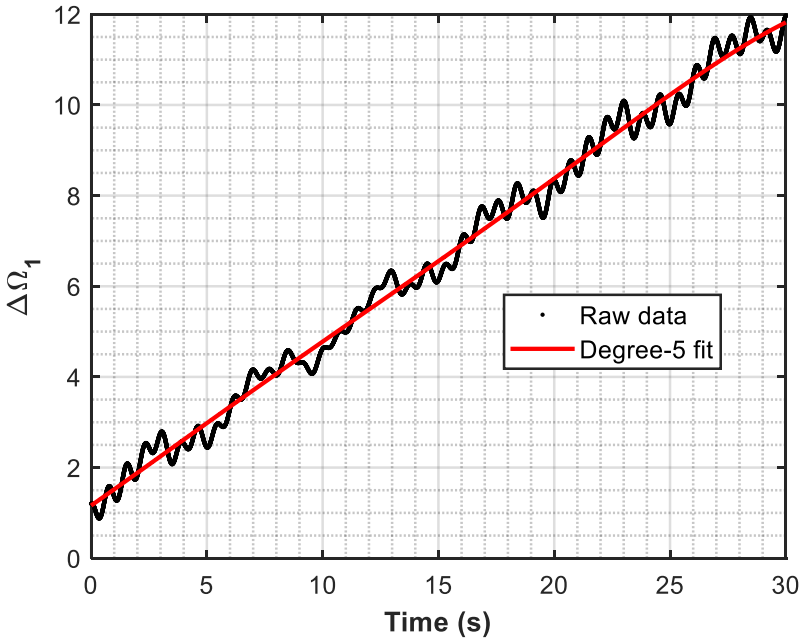


Fig. 8. Angular velocity of the low-speed input shaft (The red curve was plotted using a fifth-degree polynomial regression).

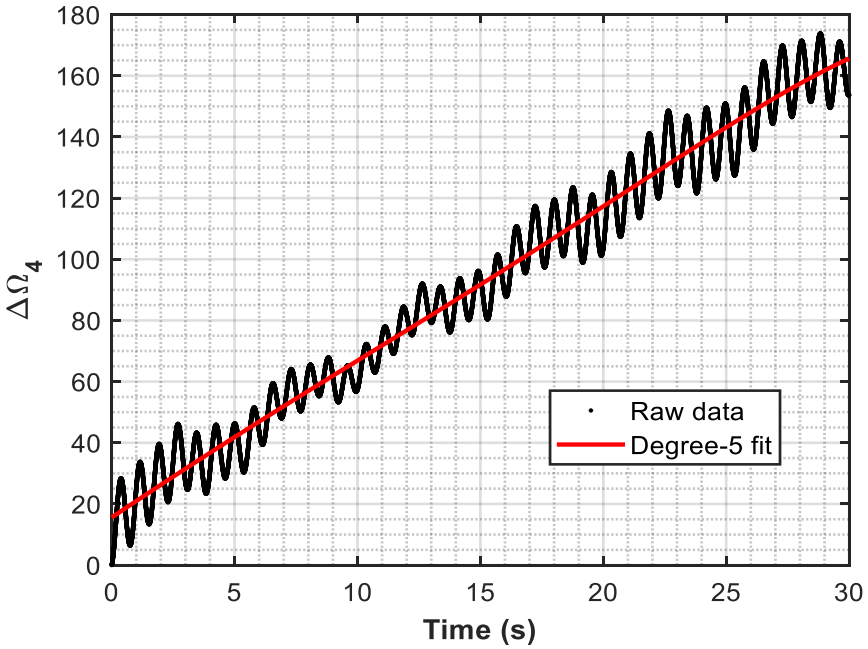


Fig. 9. Angular velocity of the output shaft connected to the generator.

For comparison purposes, the angular velocity fluctuations of all components in the powertrain are superimposed in the following analysis. As can be seen (Figure 10), the amplitude of these fluctuations gradually increases towards the generator. This behavior is predictable, as dynamic excitations and vibrations accumulate along the powertrain due to inertia distribution and transmission dynamics. In contrast, the fluctuations in torque transmitted along the shafts show a downward trend. This attenuation is desirable as operating with lower torque variability reduces mechanical stress, thereby improving the reliability and durability of the transmission.

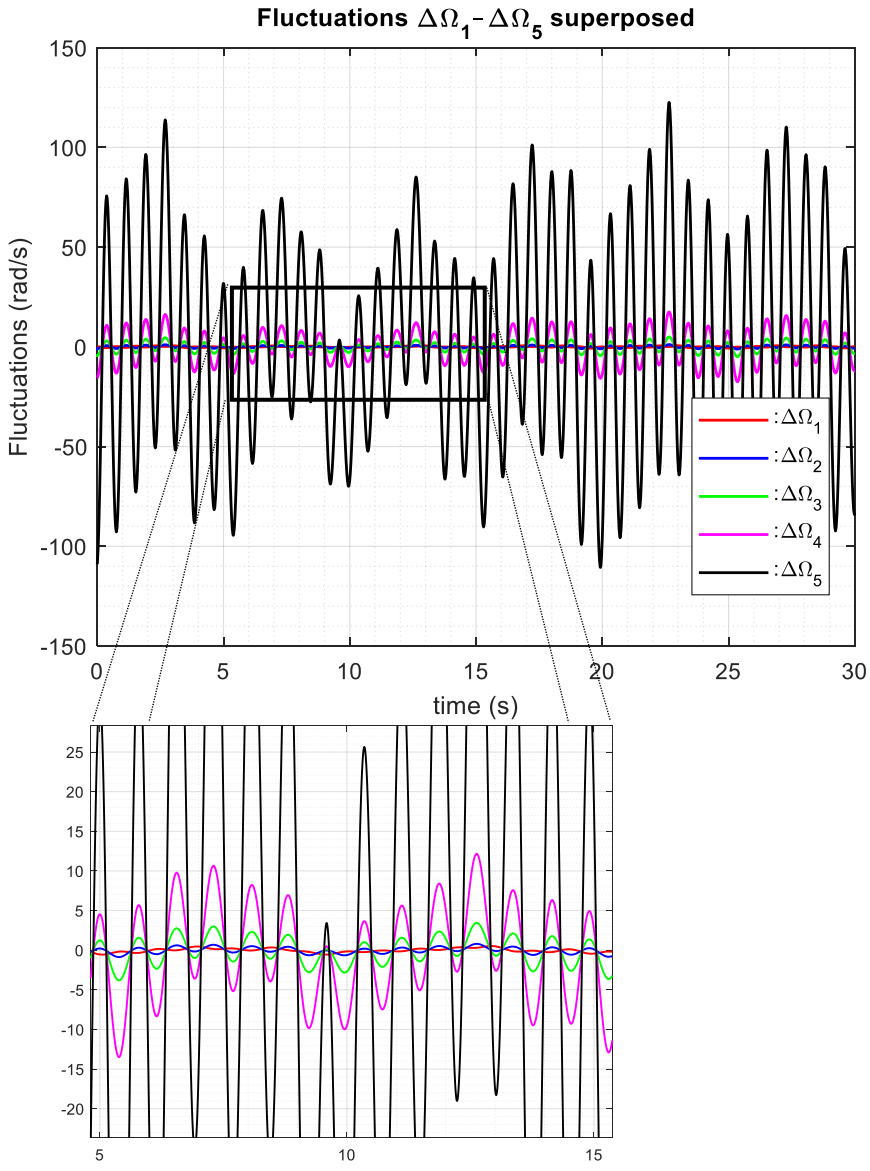
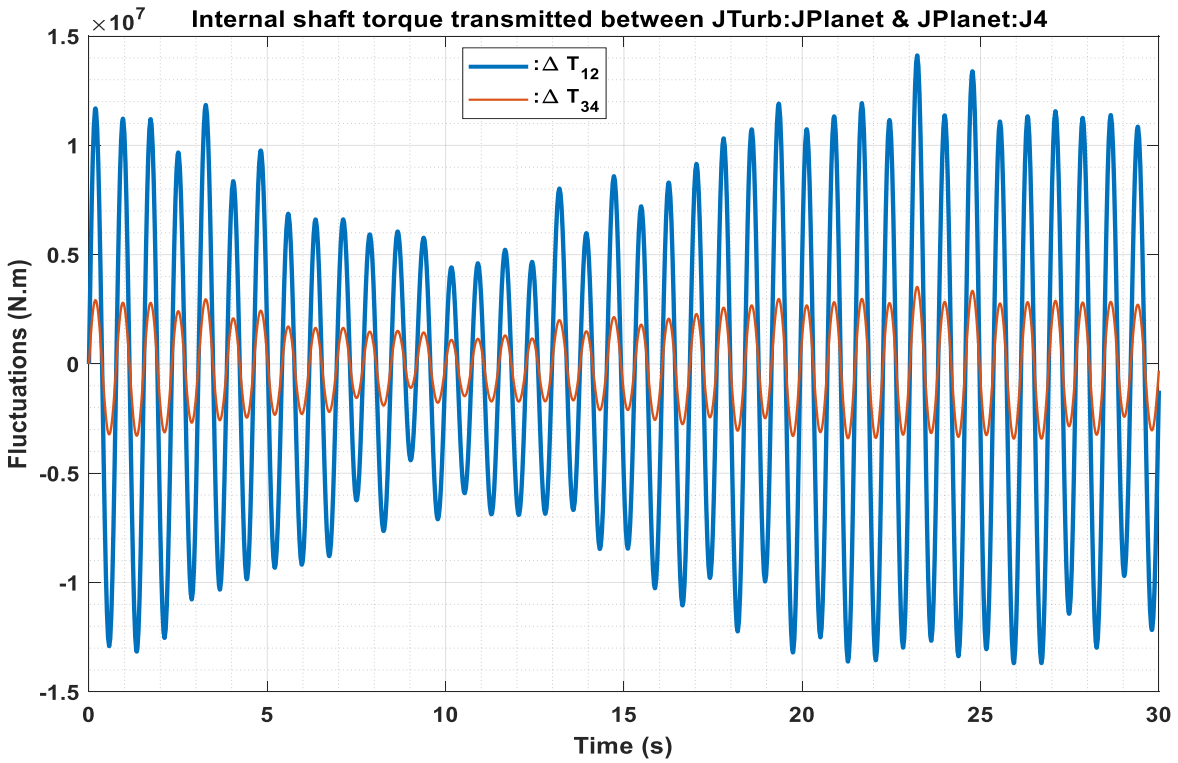


Fig. 10. Time variation of torque and rotational speed.

The figure 11 illustrate the torque fluctuations between the various shafts of the wind turbine. As one approaches the generator, it can be seen that the amplitude of these fluctuations gradually decreases, indicating that the kinematic chain attenuates these dynamic variations along its entire length.

As can be seen from the preceding figures, the dynamic behaviour of the 1.5 MW wind turbine is predominantly influenced by the input power extracted from the wind. By applying probabilistic methods, we identified a boundary that separates the safe operating region from the risk region. This facilitates the implementation of a power control strategy that depends on the wind speed measured by the anemometer and the relative orientation of the airflow with respect to each blade.

The variability in external excitation experienced by wind turbine generators is primarily due to stochastic wind conditions characterized by multidirectional flow and frequent gusts. Consequently, the gearbox must be designed to withstand the transmitted loads and the highest stochastic forces. These random, wind-induced loads can contribute to fatigue and reduce the operational lifespan of the wind turbine system as a whole. In this context, let X1 and X2 denote mutually independent, normally distributed random variables such that $X_1 \sim N(\mu_1,\sigma_1)$ [m/s] and $X_2 \sim N(\mu_2,\sigma_2)$ [degree].



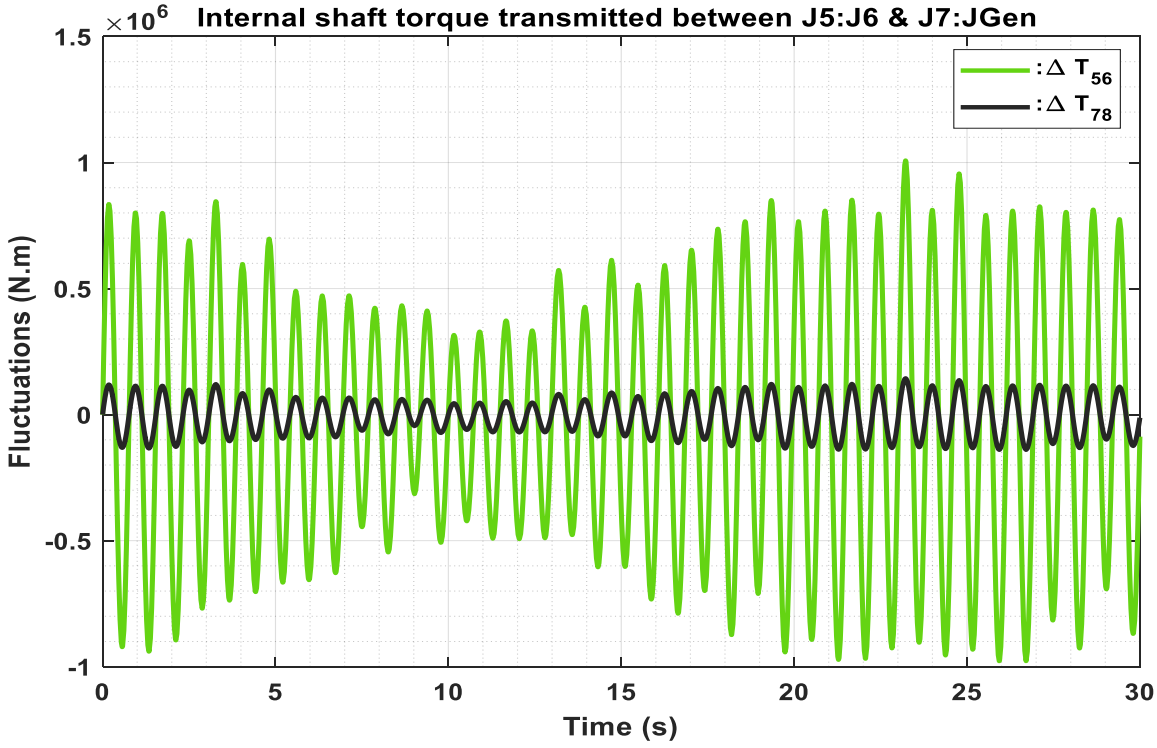


Fig. 11. Torque on the internal shafts.

Frequency Analysis and Mode Shape Normalization

The reduced-order formulation can be described using five generalized angular coordinates, each of which is associated with one of the five equivalent inertias. Consequently, the system exhibits five modal solutions, including one rigid-body mode and four elastic torsional modes. Frequency analysis was subsequently performed by solving the generalized eigenvalue problem of the undamped drivetrain system.

$$\left(\mathrm{K}-\omega_{\mathrm{n}}^{2}\mathrm{M}\right)\Phi_{\mathrm{n}}=0 \tag{28}$$

where M and K denote the mass and stiffness matrices, respectively, ω_n is the n-th natural angular frequency, and Φ_n is the corresponding mode shape. The natural frequencies were then obtained from:

$$\mathrm{f}_{\mathrm{n}}=\frac{\omega_{\mathrm{n}}}{2\pi} \tag{29}$$

The computed eigenvectors were first mass-normalized according to:

$$\Phi_n^T M \Phi_n = 1 \tag{30}$$

For a clearer visualization and interpretation of the relative modal displacements, the mode shapes were subsequently normalized with respect to their maximum absolute amplitude:

$$\hat{\Phi}_n = \frac{\Phi_n}{\max_j \left| \Phi_{jn} \right|} \tag{31}$$

Accordingly, the maximum absolute component of each normalized mode shape is equal to unity, while all remaining modal components lie within the interval:

$$-1 \le \hat{\Phi}_{jn} \le 1 \tag{32}$$

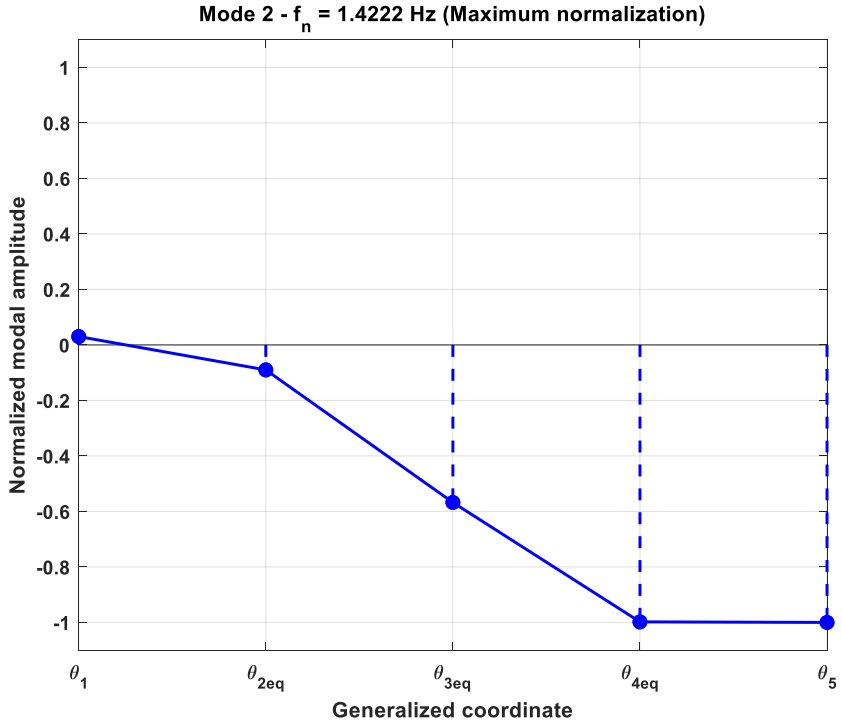
This normalization does not modify the physical characteristics of the eigenmodes but facilitates the identification of the dominant generalized coordinates and the relative phase relationships between the different drivetrain components.

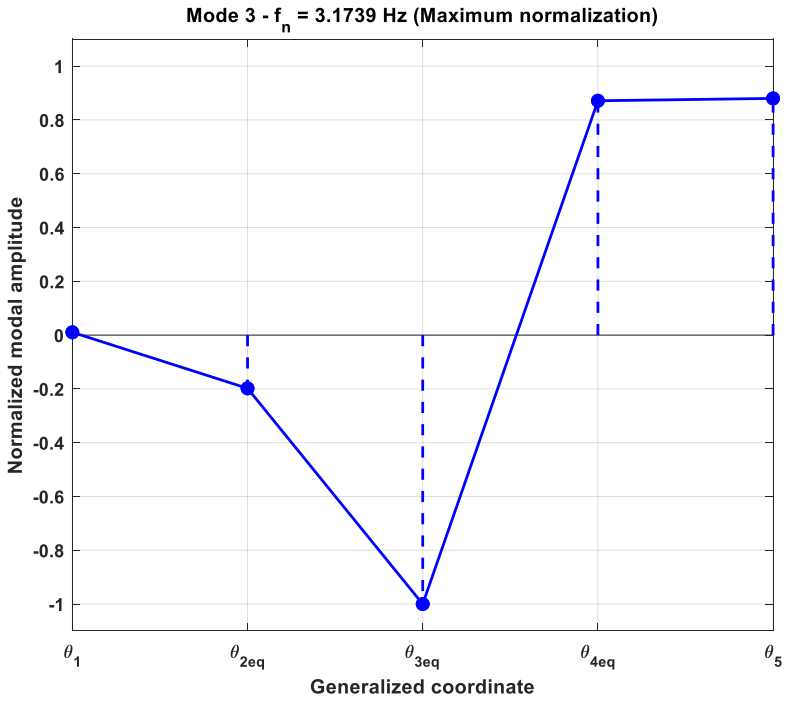
The table 4 reveals that the maximum-amplitude, normalized mode shapes clearly show the evolution of the torsional dynamics of the reduced drivetrain. Mode 1 corresponds to rigid-body rotation because all five equivalent inertias exhibit identical angular displacement. Modes 2 and 3 are global and internal torsional modes, respectively, characterized by opposite-phase motion between different equivalent inertias. In contrast, mode 4 is predominantly localized around the second equivalent inertia, and mode 5 is mainly dominated by the fifth equivalent inertia.

Table 4. Maximum amplitude normalized torsional mode shapes

Generalized angular coordinate	**Mode 1**	**Mode 2**	**Mode 3**	**Mode 4**	**Mode 5**
θ_1	1.000	0.030	0.010	-0.002	~0
θ_{2eq}	1.000	-0.090	-0.198	1.000	~0
θ_{3eq}	1.000	-0.568	-1.000	-0.017	~0
θ_{4eq}	1.000	-0.998	0.871	~0	-0.003
θ_5	1.000	-1.000	0.880	~ 0	1.000

Figure 12 presents the maximum-amplitude-normalized torsional mode shapes of the five-inertia reduced drivetrain model. Each shape illustrates the angular motion of the five inertias at their respective natural frequencies, highlighting their amplitudes and phase relationships.





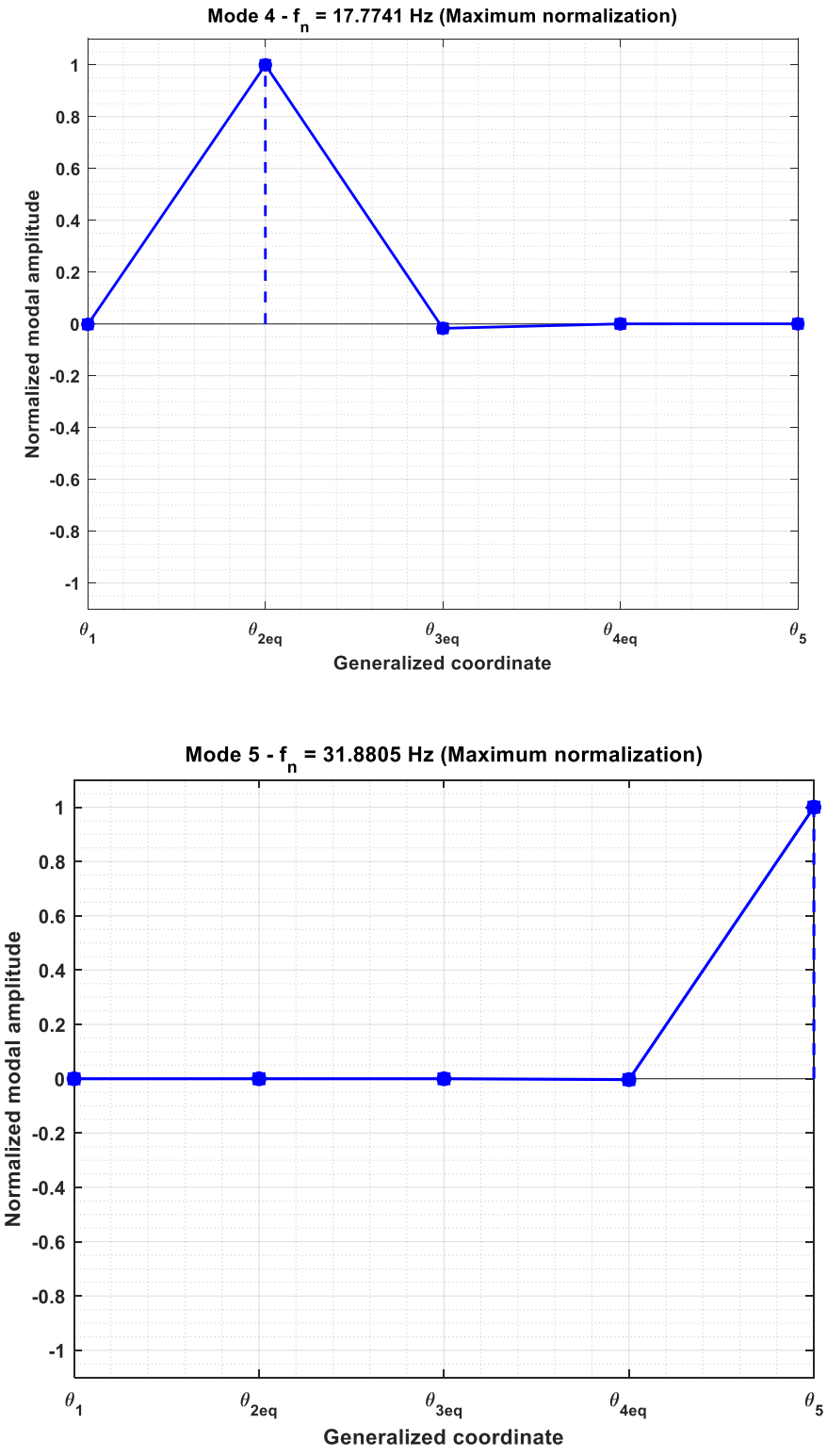


Figure 12. Normalized Torsional Mode Shapes of the Reduced Wind Turbine Drivetrain.

The reduced drivetrain model's modal characteristics are summarized in Table 5. This includes the identified physical modes, their corresponding natural frequencies, and their main dynamic characteristics. A concise overview of the transition from the rigid-body mode to the different elastic torsional modes is provided.

Table 5. Modal characteristics of the reduced wind turbine drivetrain model

Physical Mode	Natural Frequency (Hz)	Main Characteristics
Rigid-body mode	**0.000**	Global rigid rotation of the entire drivetrain without relative torsional deformation.
Elastic torsional mode 2	**1.422**	Low-frequency global torsional mode involving the relative motion between the turbine and the remaining drivetrain components.
Elastic torsional mode 3	**3.174**	Internal torsional mode characterized by opposite-phase motion between the intermediate and high-speed drivetrain sections.
Elastic torsional mode 4	**17.774**	Localized torsional mode predominantly associated with the generalized coordinate θ2eq.
Elastic torsional mode 5	**31.880**	High-frequency localized torsional mode predominantly governed by the generator coordinate θ5.

Conclusion

This study developed an integrated probabilistic–dynamic approach to investigate the reliability and dynamic behavior of a wind turbine drivetrain under uncertain aerodynamic excitation. The proposed methodology combines a blade-based aerodynamic model, a multistage lumped-parameter drivetrain model, and three complementary reliability techniques, namely FORM, SORM, and Monte Carlo Simulation. Wind speed and inflow angle were considered as the main sources of aerodynamic uncertainty, and their effects were evaluated through a torque-based limit-state function.

The reliability analysis identified critical aerodynamic conditions associated with the onset of the limit state, with a critical combination close to 11 m/s wind speed and 16° inflow angle. The failure probability was found to be strongly dependent on the assumed stochastic characteristics of the wind parameters, reaching values between 0.0145 and 0.1642. The close agreement between FORM, SORM, and Monte Carlo results confirms the consistency of the proposed probabilistic assessment.

The dynamic analysis further demonstrated that aerodynamic uncertainties directly affect the torsional behavior of the transmission. Rotational-speed fluctuations increase toward the generator, while torque fluctuations are progressively attenuated through the drivetrain. The modal analysis revealed one rigid-

body mode and four elastic torsional modes, with natural frequencies ranging from 1.422 to 31.880 Hz, providing additional insight into the vibratory characteristics of the transmission system.

Overall, the results demonstrate the benefit of coupling reliability analysis with drivetrain dynamics rather than treating aerodynamic uncertainty and mechanical response independently. The proposed framework can therefore provide a useful basis for reliability-oriented drivetrain design, critical operating-condition identification, and risk-informed maintenance strategies. Future developments should incorporate additional mechanical uncertainties, nonlinear gear interactions, and extreme or transient wind events to improve the predictive capability of the proposed approach.

Data Availability

The datasets generated and/or analysed during the current study are available from the corresponding author upon reasonable request.

References

1. Wojtaszek, H., Borowski, P. F., Handschke, M., Miciuła, I., Stecyk, A., Bielawa, A., ... & Czepło, F. (2025). Wind Energy in Transition: Development, Socio-Economic Impacts, and Policy Challenges in Europe. Energies, 18(11), 2811.
2. Jørgensen, B. H., & Holttinen, H. (2022). IEA wind TCP annual report 2021. IEA.
3. Lee, J., & Zhao, F. (2021). GWEC. Global wind report 2021.
4. Nejad, A. R., Keller, J., Guo, Y., Sheng, S., Polinder, H., Watson, S., et al. (2022). Wind turbine drivetrains: State-of-the-art technologies and future development trends. Wind Energy Science, 7, 387–411.
5. Liu, X., Wu, Z., Yuan, Y., Sun, W., & Gao, J. (2025). Reliability modeling of wind turbine Gearbox system considering failure correlation under shock–degradation. Sensors, 25(14), 4425.
6. Remigius, W. D., & Natarajan, A. (2022). A review of wind turbine drivetrain loads and load effects for fixed and floating wind turbines. Wiley Interdisciplinary Reviews: Energy and Environment, 11(1), e417.
7. Ghorbel, A., Graja, O., Hentati, T., Abdennadher, M., Walha, L., & Haddar, M. (2020). The effect of the brake location and gear defects on the dynamic behavior of a wind turbine. Arabian Journal for Science and Engineering, 45(7), 5421-5433.
8. Teng, D., Feng, Y. W., Chen, J. Y., & Lu, C. (2022). Structural dynamic reliability analysis: review and prospects. International Journal of Structural Integrity, 13(5), 753-783.
9. Llopis-Albert, C., Rubio, F., Devece, C., & García-Hurtado, D. (2024). Digital twin-based approach for a multi-objective optimal design of wind turbine gearboxes. Mathematics, 12(9), 1383.
10. Li, Z., Wen, B., Peng, Z., Dong, X., & Qu, Y. (2020). Dynamic modeling and analysis of wind turbine drivetrain considering the effects of non-torque loads. Applied Mathematical Modelling, 83, 146-168.
11. Moghadam, F. K., Rebouças, G. F. D. S., & Nejad, A. R. (2021). Digital twin modeling for predictive maintenance of gearboxes in floating offshore wind turbine drivetrains. Forschung im Ingenieurwesen, 85(2), 273-286.
12. Bacem, Z., Imen, B., Kamel, A., Lassaad, W., & Mohamed, H. (2022). Study of dynamic behavior of a bevel gear used in vertical axis wind turbine. Journal of the Chinese Society of Mechanical Engineers, 43(5), 569-577.

13. Abboudi, K., Walha, L., Driss, Y., Maatar, M., Fakhfakh, T., & Haddar, M. (2011). Dynamic behavior of a two-stage gear train used in a fixed-speed wind turbine. Mechanism and Machine theory, 46(12), 1888-1900.
14. Karmi, B., Saouab, A., Guerine, A., Bouaziz, S., Hami, A. E., Haddar, M., & Dammak, K. (2024). Reliability based design optimization of a two-stage wind turbine gearbox. Mechanics & Industry, 25, 16.
15. Chen, R., Qin, D., & Liu, C. (2023). Dynamic modelling and dynamic characteristics of wind turbine transmission gearbox-generator system electromechanical-rigid-flexible coupling. Alexandria Engineering Journal, 65, 307-325.
16. Yang, S., & Chen, Y. (2025). Modelling and analysis of offshore wind turbine gearbox under multi-field coupling. International Journal of Ocean Systems Management, 2(1), 52-66.
17. Xue, Z., Zhang, H., & Ji, Y. (2023). Dynamic Response of a Flexible Multi-Body in Large Wind Turbines: A Review. Sustainability, 15(8), 6590.
18. Yang, S., Zhu, C., Li, C., Zhou, Y., Tan, J., & Liao, B. (2025). Physics-data hybrid dynamic analysis of novel integrated wind turbine drivetrain. International Journal of Mechanical Sciences, 110564.
19. Ghorbel, A., Graja, O., Bouaziz, A., Abdennadher, M., Walha, L., & Haddar, M. (2019, June). Parametric Study of a Minimal Model of Wind Turbine Drivetrain System. In International Conference Mechatronics (pp. 125-132). Cham: Springer International Publishing.
20. Didier, F., Liu, Y. C., Laghrouche, S., & Depernet, D. (2024). A comprehensive review on advanced control methods for floating offshore wind turbine systems above the rated wind speed. Energies, 17(10), 2257.
21. Zghal, B., Bel Mabrouk, I., Walha, L., Abboudi, K., & Haddar, M. (2019). Analyses of dynamic behavior of vertical Axis wind turbine in transient regime. Advances in Acoustics and Vibration, 2019(1), 7015262.
22. Tounsi, M., Beyaoui, M., Abboudi, K., Feki, N., Walha, L., & Haddar, M. (2016). Influence of uncertainty in aerodynamic performance on the dynamic response of a two stage gear system. Journal of Theoretical and Applied Mechanics, 54(2), 601-612.
23. Hadj Kacem, M., El Hami, A., Dammak, K., Trabelsi, H., Walha, L., & Haddar, M. (2024). Consideration of multi-variable uncertainty using the GPC method for the dynamic study of a two-stage gearbox of a wind turbine. Mechanics of Advanced Materials and Structures, 31(7), 1464-1477.
24. Su, C., Wu, J., Jiang, G., Zhang, N., & Song, X. (2023). Uncertainty analysis of wind speed of wind turbine. Quality and Reliability Engineering International, 39(5), 1814-1830.
25. Li, H., Cho, H., Sugiyama, H., Choi, K. K., & Gaul, N. J. (2017). Reliability-based design optimization of wind turbine drivetrain with integrated multibody gear dynamics simulation considering wind load uncertainty. Structural and multidisciplinary optimization,56(1), 183-201.
26. Gonzaga, P., Toft, H., Worden, K., Dervilis, N., Bernhammer, L., Stevanovic, N., & Gonzales, A. (2022). Impact of blade structural and aerodynamic uncertainties on wind turbine loads. Wind Energy, 25(6), 1060-1076.
27. Sarbandi, M., & Khaloozadeh, H. (2024). Quantifying the impact of sensor precision on power output of a wind turbine: A sensitivity analysis via Monte Carlo simulation study. Wind Engineering, 48(4), 497-517.
28. Mazetto, B. M., & Ritto, T. G. (2022). Uncertainty and global sensitivity analysis of wind turbines fatigue in non-ideal conditions. Journal of Vibration Engineering & Technologies, 10(6), 2391-2402.
29. Du, H., Tan, J., Li, H., Fei, W., & Sun, Z. (2025). Numerical modeling and analysis of multistage gear transmission system in wind turbine gearbox under load uncertainty. Proceedings of the

Institution of Mechanical Engineers, Part C: Journal of Mechanical Engineering Science, 239(3), 767–788.
30. Gu, H., Wang, H., Zhou, J., Fei, X., Wen, J., & Fang, Z. (2025). System dynamic reliability of wind turbine gearbox under random wind load. Journal of Vibration and Shock, 44(3), 238–250.

Funding
This research did not receive funding.

Author contributions

Kamel Abboudi: Conceptualization, Methodology, Writing – original draft. Ahmed Ghorbel: Conceptualization, Methodology. Mohanad Bahshwan: Conceptualization, Methodology. Sami Ghazali: Methodology, Validation. Ali Mkaddem: Investigation, Data curation. Abdessalem Jarraya: Conceptualization, Supervision, Project administration. Mohamed Haddar: Writing – review & editing. All authors contributed to the discussion and interpretation of the results, reviewed the manuscript, and approved the final version of the manuscript.

Competing interests

The authors declare no competing interests.

Correspondence

Correspondence and requests for materials should be addressed to Abdessalem Jarraya.